Available online at www.sciencedirect.com

ScienceDirect

Ceramics International 40 (2014) 3149–3154

CERAMICS INTERNATIONAL

www.elsevier.com/locate/ceramint

Generalized synthesis of yolk–shell metal oxide spheres

Hongfang Jiu[a,*], Yixin Sun[b], Lixin Zhang[b], Chaoyan Zhang[b], Jia Zhang[b], Jianwei Liu[c]

[a]College of Science, North University of China, Taiyuan 030051, PR China
[b]Chemical Engineering and Environmental Institute, North University of China, Taiyuan 030051, PR China
[c]Department of Physics and Astronomy, University of Kansas, 1082 Malott Hall, Lawrence, KS 66045, USA

Received 7 September 2013; received in revised form 26 September 2013; accepted 27 September 2013
Available online 7 October 2013

Abstracts

Varieties of yolk–shell metal oxide spheres, including SnO_2, CeO_2 and Tb_4O_7, with high yield have been successfully prepared *via* a general solvothermal method by using carbon spheres as sacrificial templates. The creation of yolk–shell structure is achieved after the removal of carbon templates by annealing. The results show that the typical products of yolk–shell SnO_2 spheres exhibit excellent textural properties, which makes them good candidates for use in gas-sensing, energy storage, and so on. Many more metal oxides with such a unique yolk–shell structure can be easily prepared through the present approach, and they may show great application potentials.
© 2013 Elsevier Ltd and Techna Group S.r.l. All rights reserved.

Keywords: A. Calcination; B. Porosity; C. Thermal properties; D. Sensors; Powders: chemical preparation

1. Introduction

The creation of microscopic materials has experienced a great structural evolution from simple to complex with the development of modern synthesis technology and analytical instruments because materials always show a strong correlation between their geometry and their functions [1–3]. For instance, in addition to general solid materials, the creation of hollow materials has become a critical issue in recent years owing to their great advantages of large void space area fraction, low density and special shape, which generally results in enhanced properties and novel application potentials compared to solid particles [4–10]. For the sake of further enhancing the properties and extending the applications of materials, their preparation with novel structures has attracted significant attention [11–16]. For instance, compared to the general hollow spheres, metal oxides with unique yolk–shell (hollow core–shell) and multiple shell hollow structure exhibit greatly enhanced gas-sensing properties [17].

Owing to the potential of their emerging applications spanning from catalyst, sensors, and microelectronic devices, to energy conversion devices including solar and fuel cells, nanoscale metal oxides are of tremendous current interest to scientists and engineers [18,19]. For example, Tin oxide (SnO_2) with an n-type wide bandgap equal to 3.6 eV is a functional material widely applied in gas-sensing and energy storage [20–23]. Cerium(IV) oxide (CeO_2), as one of the most important catalysts, has also attracted much research interest because of its effective technological applications [24,25]. Terbium(III,IV) oxide (Tb_4O_7), a typical rare earth oxide, may also show great application potentials in drug delivery systems and so on [26].

Previously, by using a solvothermal carbon template method, we have prepared yolk–shell $ZnCo_2O_4$ spheres. Herein, we further present the general synthesis of a series of metal oxides, including SnO_2, CeO_2, and Tb_4O_7, with unique yolk–shell structure through a similar approach. The results show that the typical products of yolk–shell SnO_2 spheres exhibit excellent properties, which promise great potential in technical applications.

2. Methods and materials

2.1. Materials

Glucose was purchased from Tianjin Co., Ltd. (Tianjin). Tb_2O_3, $Ce(NO_3)_3 \cdot 6H_2O$ and $NH_4Ac \cdot 2H_2O$ were purchased from Yuanli Co., Ltd. (Tianjin). $SnCl_2 \cdot 2H_2O$ was purchased from Kermel Co., Ltd. (Tianjin). N,N-Dimethylformamide (DMF) was purchased

*Corresponding author. Tel.: +86 351 3923197.
E-mail address: hfjiu@126.com (H. Jiu).

0272-8842/$ - see front matter © 2013 Elsevier Ltd and Techna Group S.r.l. All rights reserved.
http://dx.doi.org/10.1016/j.ceramint.2013.09.129

from Tianli Co., Ltd. (Tianjin). Concentrated HCl and HNO_3 were purchased from Tianda Co., Ltd. (Tianjin). All chemical materials were used as received.

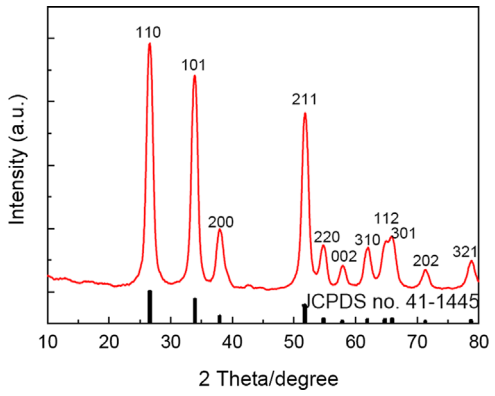

Fig. 1. XRD pattern of resultant yolk–shell SnO_2 spheres.

2.2. Synthesis

2.2.1. Preparation of yolk–shell SnO_2 spheres

Carbon spheres with an average particle size of 500 nm were prepared according to a present method and used as templates to direct the synthesis of yolk–shell metal oxide spheres [27]. For the synthesis of yolk–shell SnO_2 spheres, a suspension was made after dissolving 0.1 g $SnCl_2 \cdot 2H_2O$ in a mixture containing 25.0 mL DMF, 5.0 mL H_2O and 0.5 mL concentrated HCl (37%) followed by the dispersion of 0.3 g as-prepared carbon spheres. The suspension was transferred into a 50 mL Teflon-linked autoclave, and it was maintained at 180 °C for 12 h. Black precipitates were separated from the mixture and were dried at 100 °C. The black precipitate was further heated to 600 °C with a temperature ramp of 5 °C min^{-1} and kept at the same temperature for 3 h in air, and the yolk–shell SnO_2 spheres were formed.

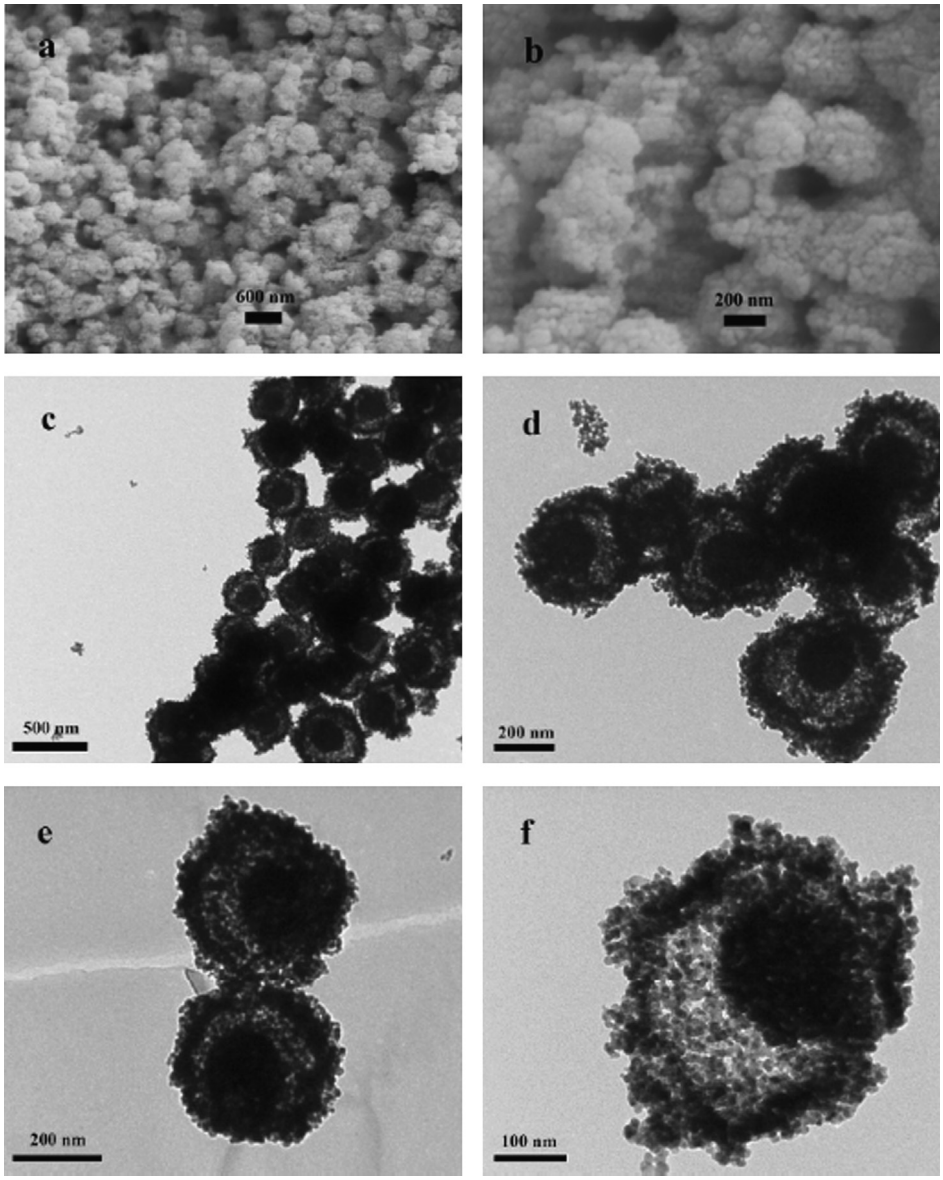

Fig. 2. FESEM (a, b) and TEM (c)–(f) images of yolk–shell SnO_2 spheres.

2.2.2. Preparation of yolk–shell CeO_2 and Tb_4O_7 spheres

Taking the synthesis of yolk–shell CeO_2 spheres for example, a black suspension was obtained after dissolving 0.2 g Ce $(NO_3)_3 \cdot 6H_2O$, 1.0 g PVP and 0.5 g $NH_4Ac \cdot 2H_2O$ in 30.0 mL absolute ethanol followed by dispersing 0.3 g as-prepared carbon spheres. The suspension was transferred into a 50 mL Teflon-linked autoclave, and it was maintained at 180 °C for 12 h. Black precipitates were separated from the mixture and were dried at 100 °C. Final products were prepared after annealing the black precipitates at 600 °C for 3 h in air.

For the preparation of yolk–shell Tb_4O_7 spheres, $Tb(NO_3)_3$ crystals were prepared from dissolving purchased Tb_2O_3 in concentrated HNO_3 after complete removal of solvent and nitric acid, and the crystals were used as the metal source. Yolk–shell Tb_4O_7 spheres were prepared under the same synthesis conditions except for the addition of PVP.

2.3. Measurements and characterizations

The phase and purity of samples was determined by using Japan D/max-rB X-ray diffraction (XRD). The morphology and structure measurements were conducted by a Japan Hitachi S-4800 field emission scanning electron microscope (FESEM) and a Japan JEOL JEM-1400 microscope (TEM), respectively. The thermo-gravimetric–differential thermoanalysis (TG–DTA) properties were recorded by China ZCT-2000 thermo-gravimetric analysis. The surface area and pore size distribution were measured through nitrogen adsorption–desorption analyzed on a USA Micromeritic ASAP 2020 nitrogen adsorption apparatus.

3. Results and discussions

The preparation of yolk–shell metal oxide spheres, similar to our previous work, can be described as follows. The carbon spheres with a large number of mesopores were used as templates. During the solvothermal, the metal source was first converted to nucleates, and these nucleates were loaded into the mesopores within templates driven by the vigorous internal thermal motion of molecules. Then, after the complete removal of template by calcination, the creation of yolk–shell structure was achieved. The details of formation mechanism are shown in Ref. [28].

The crystallinity and the phase purity of resultant yolk–shell SnO_2 spheres were examined by XRD, and the results are presented in Fig. 1. Fig. 1 indicates that all the diffraction peaks can be very well indexed to tetragonal phase of SnO_2 (space group P42/mnm (136) with cell constants $a=b=4.738$ Å and $c=3.187$ Å, JCPDS no. 41-1445), suggesting that the resultant yolk–shell SnO_2 spheres have a perfect rutile crystalline lattice. In addition, the mean crystalline size of the SnO_2 nanocrystals has also been calculated to be approximately 11.22 nm by using Scherer's formula [29]. The calculated grain size is in good agreement with that of TEM observations, as shown in Fig. 2f.

The FESEM observations of the resultant yolk–shell SnO_2 spheres, as shown in Fig. 2a and b, show the spherical morphology

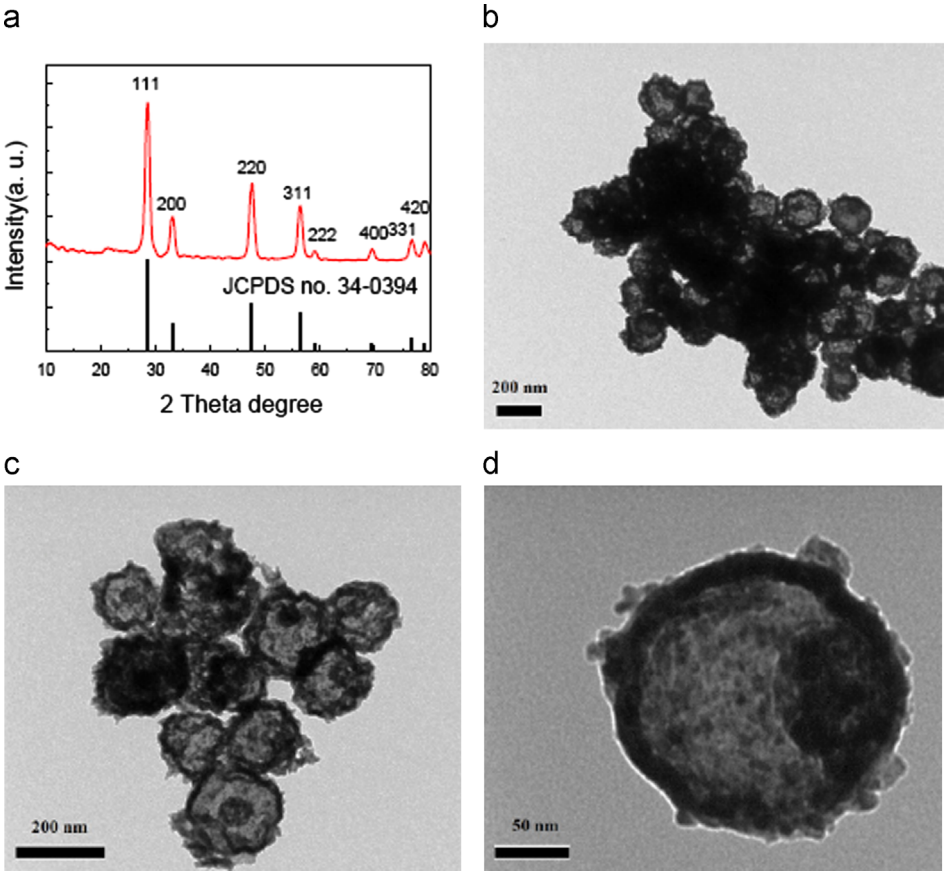

Fig. 3. XRD pattern (a) and TEM images (b)–(d) of as-synthesized yolk–shell CeO_2 spheres.

of particles with a uniform particle size of 420 nm. Particularly, in Fig. 2b, crashed spheres holding a movable core clearly suggest the yolk–shell structure of sample. However, one can also conclude that the yolk–shell spheres consist of a large amount of small particles. Fig. 2c–f further illustrates the TEM images of resultant yolk–shell SnO_2 spheres. The TEM images show obvious contrast between the dark edges and the pale intervals, providing convincing evidence of the hollow nature of sample. A relatively smaller particle is encapsulated into a bigger one to generate the yolk–shell structure. The shells of such unique yolk–shell spheres are composed of a large number of small nanoparticles with an average diameter of 11.4 nm, as shown in Fig. 2f. However, the yolk–shell spheres possess an average particle size of approximately 430 nm, which is much smaller than that of templates, and the shrinkage is attributed to the dense of precursor during calcination [30].

As mentioned, yolk–shell CeO_2 and Tb_4O_7 spheres have also been prepared through a similar approach, and they were characterized through XRD and TEM. In Fig. 3, the XRD pattern (a) and TEM images (b–d) of as-synthesized yolk–shell CeO_2 spheres are exhibited. All the diffraction peaks in Fig. 3a can be readily indexed to the cubic phase CeO_2 (space group Fm-3m(225) with a lattice constant $a=5.411$ Å, JCPDS card no. 34-0394). In Fig. 3b–d, the strong contrast between the dark edges and pale intervals of particles provides a convincing evidence of the yolk–shell structure of sample. Similarly, the shells of yolk–shell CeO_2 spheres are composed of a large number of small nanoparticles, and they also possess an average particle size of approximately 180 nm, which is much smaller than that of the templates.

Fig. 4 further shows the XRD pattern (a) and TEM observations (b–d) of as-prepared yolk–shell Tb_4O_7 spheres. As shown in Fig. 4a, all the characteristic peaks can be assigned to cubic phase Tb_4O_7 (face-center with a cell constant $a=5.315$ Å, JCPDS card no. 32-1286). Any other peak is not found, suggesting the high purity of sample. The yolk–shell structure of sample is also confirmed according to the strong contrast between the dark edges and pale centers shown in Fig. 4b–d. The spheres exhibit an average particle size of approximately 200 nm. However, compared to the yolk–shell SnO_2 and CeO_2 spheres, the as-prepared yolk–shell Tb_4O_7 spheres possess a much smoother surface.

As a typical example, the thermogravimetric (TG) and differential thermoanalysis (DTA) curves of C–SnO_2 are presented in Fig. 5. It can be concluded from Fig. 5 that weight loss includes three steps. In detail, the weight loss occurring from 50 °C to 200 °C is resulted by the loss of free water. However, the weight loss occurring from 200 °C to 400 °C and the weight loss occurring between 400 °C and 600 °C, corresponding to the two major exothermic peaks, can be attributed to the removal of carbon spheres templates by different strategies. Similar to previous works, the isolated exothermic peaks may suggest the different combustion kinetics of template, corresponding to the shell forming and core forming steps [27,31]. Any further weight

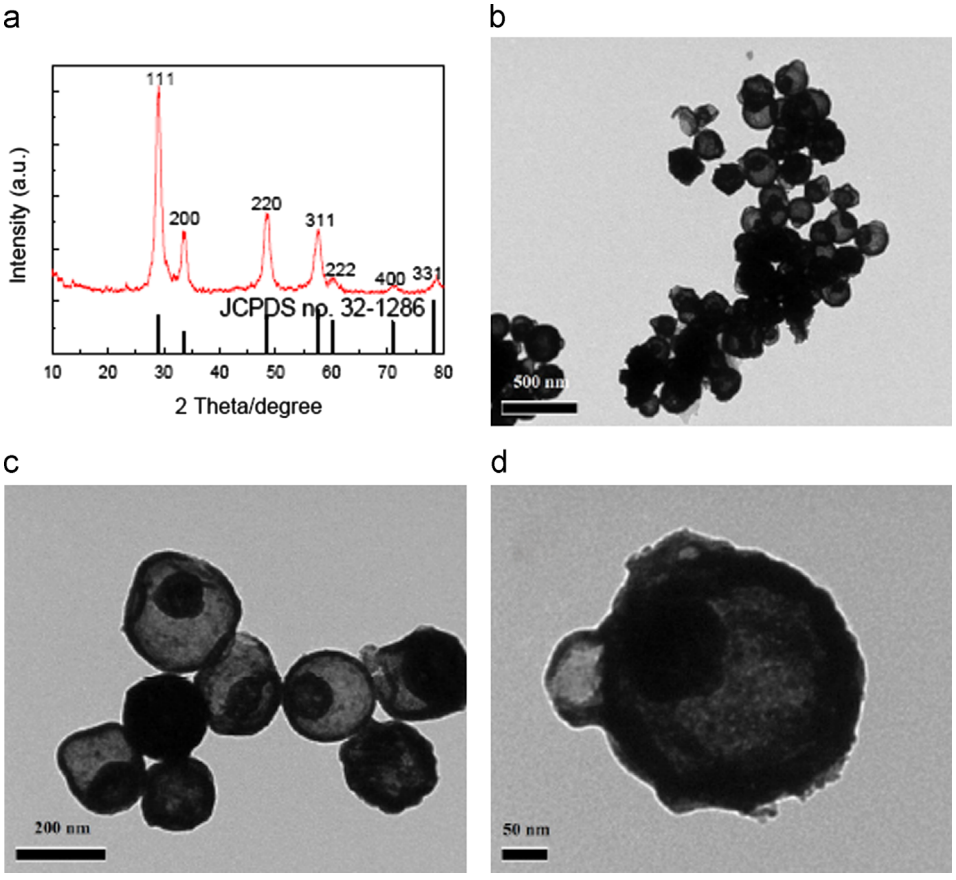

Fig. 4. XRD pattern (a) and TEM images (b)–(d) of as-synthesized yolk–shell Tb_4O_7 spheres.

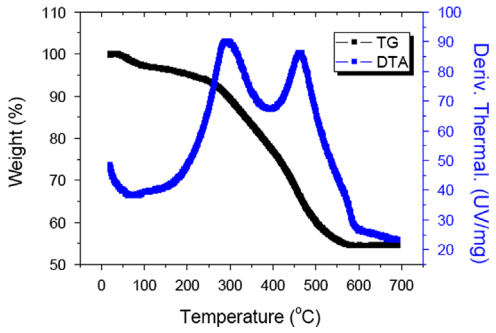

Fig. 5. TG–DTA curves of C–SnO_2 composites.

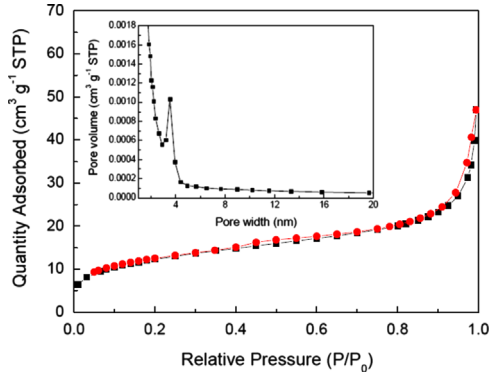

Fig. 6. Nitrogen sorption isotherm and pore size distribution (inset) of yolk–shell SnO_2 spheres.

loss and exothermic peak over 600 °C are not found, revealing that the carbon templates must have been removed completely. The weight of precursor absorbed is measured to be more than 55%, which is extremely high. The high adsorption efficiency is attributed to the complete conversion of metal source to precursor and the complete loading of them into mesopores within templates driven by solvothermal. In addition, the high adsorption efficiency may suggest that the present method can prevent in the preparing process the potential wasting of materials and pollution because very few metal was left in the solution.

Fig. 6 shows the nitrogen sorption isotherm and pore size distribution (inset) of typical products of resultant yolk–shell SnO_2 spheres. It can be concluded that the isotherm has type IV characteristics and a type H3 loop with a narrow pore size distribution in mesoporous region [32]. The specific surface area of resultant yolk–shell SnO_2 spheres calculated from the sorption isotherm is 42.87 $m^2\ g^{-1}$. As shown in the inset, a narrow pore size of sample is distributed around 3–4 nm. The average pore size of sample, which is approximately 6.8 nm, is calculated from the desorption branch of the isotherm using the BJH method. The curve of pore volume distribution against pore size in Fig. 6 inset clearly shows that the sample possesses a high total pore volume, which is measured to be 0.073 $cm^3\ g^{-1}$. The high pore volume probably originated from the mesopores on the shell and particularly the hollow interior voids of intra-particles which are responsible for the sharp rises in adsorption at high pressures. The results suggest that the resultant yolk–shell SnO_2 spheres exhibiting excellent textural properties may be applied as particularly good candidates for use in catalysis, gas-sensing, and so on.

4. Conclusions

In summary, a series of metal oxides, including SnO_2, CeO_2, and Tb_4O_7, with unique yolk–shell structure have been prepared by using carbon spheres as templates. Many more yolk–shell metal oxides spheres can be easily prepared through such a general method. It is also assumed that the combination of such yolk–shell structures and porous shells of materials will enable the development of novel gas sensors, catalysts, energy storage devices and drug delivery systems.

Acknowledgments

Financial supports from the Shanxi (20110321037-02) Science and Technology Foundation of China and ShanXi (2012081020) International Science and Technology Operation of China are appreciated.

References

[1] X. Lai, J.E. Halpert, D. Wang, Recent advances in micro-/nano-structured hollow spheres for energy applications: from simple to complex systems, Energy and Environmental Science 5 (2012) 5604–5618.
[2] Y. Zhao, L. Jiang, Hollow micro/nanomaterials with multilevel interior structures, Advanced Materials 21 (2009) 1–18.
[3] W.J. Feast, F. Cacialli, A.T.H. Koch, R. Daik, C. Lartigau, R.H. Friend, D. Beljonne, J.-L. Brédas, Control of luminescence in conjugated polymers through control of chain microstructure, Journal of Materials Chemistry 17 (2007) 907–912.
[4] X.W. (David) Lou, L.A. Archer, Z. Yang, Hollow micro-/nanostructures: synthesis and applications, Advanced Materials 21 (2008) 3987–4019.
[5] G.R. Bourret, R.B. Lennox, 1D $Cu(OH)_2$ nanomaterial synthesis template in water microdroplets, Journal of the American Chemical Society 132 (2010) 6657–6659.
[6] L. Li, R.Z. Ma, N. Iyi, Y. Ebina, K. Takasa, T. Sasaki, Hollow nanoshells of layered double hydroxide, Chemical Communications 29 (2006) 3215–3217.
[7] K.J. Son, H.-J. Yoon, J.-H. Kim, W.-D. Jang, Y. Lee, W.-G. Koh, Photosensitizing hollow nanocapsules for combination cancer therapy, Angewandte Chemie International Edition 50 (2011) 11968–11971.
[8] S. Jeon, K. Yong, A novel composite hierarchical hollow structure: one-pot synthesis and magnetic properties of $W_{18}O_{49}$–WO_2 hollow nanourchins, Chemical Communications (2009) 7042–7044.
[9] K. Cheng, S.H. Sun, Recent advances in synthesis and therapeutic applications of multifunctional porous hollow nanoparticles, Nano Today 5 (2010) 183–196.
[10] X.F. Yu, D.S. Wang, Q. Peng, Y.D. Li, High performance electrocatalyst: Pt–Cu hollow nanocrystals, Chemical Communications 47 (2011) 8094–8096.
[11] Z. Dong, X. Lai, J.E. Halpert, N. Yang, L. Yi, J. Zhai, D. Wang, Z. Tang, L. Jiang, Accurate control of multishelled ZnO hollow microspheres for dye-sensitized solar cells with high efficiency, Advanced materials 24 (2012) 1046–1049.
[12] Y. Sun, B. Wiley, Z-Y. Li, Y. Xia, Synthesis and optical properties of nanorattles and multiple-walled nanoshells/nanotubes made of metal alloys, Journal of the American Chemical Society 126 (2004) 9399–9406.
[13] L. Zhou, D. Zhao, X.W. Lou, Double-shelled $CoMn_2O_4$ hollow microcubes as high-capacity anodes for lithium-ion batteries, Advanced Materials 25 (2012) 745–748.

[14] Y. Zhu, E. Kockrick, T. Ikoma, N. Hanagata, S. Kaskel, An efficient route to rattle-type Fe_3O_4@SiO_2 hollow mesoporous spheres using colloidal carbon spheres templates, Chemistry of Materials 21 (2009) 2547–2553.
[15] P. Tartaj, T. González-Carreño, C.J. Serna, Single-step nanoengineering of silica coated maghemite hollow spheres with tunable magnetic properties, Advanced Materials 13 (2001) 1620–1624.
[16] Z. Tian, Y. Zhou, Z. Li, Q. Liu, Z. Zou, Generalized synthesis of a family of multishelled metal oxide hollow microspheres, Journal of Materials Chemistry A 1 (2013) 3575–3579.
[17] X. Lai, J. Li, B.A. Korge, Z. Dong, Z. Li, F. Su, J. Du, D. Wang, General synthesis and gas-sensing properties of multiple-shell metal oxide hollow microspheres, Angewandte Chemie International Edition 50 (2011) 2738–2741.
[18] R. Sui, P. Charpentier, Synthesis of metal oxide nanostructures by direct sol–gel chemistry in supercritical fluids, Chemical Reviews 112 (2012) 3057–3082.
[19] Z. Wang, L. Zhou, X.W. (David) Lou, Metal oxide hollow nanostructures for lithium-ion batteries, Advanced Materials 24 (2012) 1903–1911.
[20] N. Shirahata, W. Shin, N. Murayama, A. Hozumi, Y. Yokogawa, T. Kameyama, Y. Masuda, K. Koumoto, Reliable monolayer-template patterning of SnO_2 thin films from aqueous solution and their hydrogen-sensing properties, Advanced Functional Materials 14 (2004) 580–588.
[21] Y.L. Wang, X.C. Jiang, Y.N. Xia, Solution-phase, precursor route to polycrystalline SnO_2 nanowires that can be used for gas-sensing under ambient conditions, Journal of the American Chemical Society 126 (2003) 16176–16177.
[22] X.W. Lou, C. Yuan, L.A. Archer, Shell-by-shell synthesis of tin oxide hollow colloids with nanostructured walls: cavity size tuning and fictionalization, Small 3 (2007) 261–265.
[23] J.S. Chen, X.W. (David) Lou, Synthesis and application in lithium-ion batteries, Small 9 (2013) 1877–1893.
[24] Z. Shao, S.M. Haile, J. Ahn, P.D. Ronney, Z. Zhan, S.A. Barnett, A thermally self-sustained micro-solid-oxide fuel-cell stack with high power density, Nature 435 (2005) 795–798.
[25] W. Deng, M. Flytzani-Stephanopoulos, On the issue of the deactivation of Au–Ceria and Pt–Ceria water–gas shift catalysts in practical fuel-cell applications, Angewandte Chemie International Edition 45 (2006) 2285–2289.
[26] M.K. Devaraju, S. Yin, T. Sato, A fast and template free synthesis of Tb: Y_2O_3 hollow microspheres via supercritical solvothermal method, Crystal Growth and Design 9 (2009) 2944–2949.
[27] X.M. Sun, Y.D. Li, Colloidal carbon spheres and their core/shell structures with nobel-metal nanoparticles, Angewandte Chemie International Edition 43 (2004) 597–601.
[28] Y. Sun, L. Zhang, J. Zhang, P. Chen, S. Xin, Z. Li, J. Liu, Synthesis of hollow core-shell $ZnCo_2O_4$ spheres and their formation mechanism, Ceramics International (2013)http://dx.doi.org/, 10.1016/j.ceramint.2013.07.048.
[29] H.J. Ahn, H.C. Choi, K.W. Park, S.B. Kim, Y.E. Sung, Investigation of the structural and electrochemical properties of size-controlled SnO_2 nanoparticles, Journal of Physical Chemistry B 18 (2004) 9815–9820.
[30] X. Sun, Y. Li, Ga_2O_3 and GaN semiconductor hollow spheres, Angewandte Chemie International Edition 43 (2004) 2831–3827.
[31] H.X. Yang, J.F. Qian, Z.X. Chen, X.P. Ai, Y.L. Cao, Multilayered nanocrystalline SnO_2 hollow microspheres synthesized by chemically induced self-assembly in the hydrothermal environment, Journal of Physical Chemistry C 111 (2007) 14067–14071.
[32] J. Yu, J.C. Yu, M.K.-P. Leung, W. Ho, B. Cheng, X. Zhao, Effects of acidic and basic hydrolysis catalysts on the photocatalytic activity and microstructures of bimodal mesoporous titania, Journal of Catalysis 217 (2003) 69–78.